Design of a noninvasive system to characterize collagen-sponge remodeling using MRI

Mohammed Salman Shazeeb[1,2], Stuart Howes[2], Sivakumar Kandasamy[2], Christopher H. Sotak[1,2], and George Pins[2]

[1]*Radiology, University of Massachusetts Medical School, Worcester, MA, United States,* [2]*Biomedical Engineering, Worcester Polytechnic Institute, Worcester, MA, United States*

Introduction: The *in vivo* evaluation of the remodeling of soft biomaterial implants often involves surgical removal of the implant for subsequent histological assessment [1]. This approach is very resource intensive, it is often destructive, and imposes practical limitations on how effectively these materials can be evaluated. Magnetic resonance imaging (MRI) has the potential to non-invasively monitor the remodeling of collagen scaffolds, specifically the biodegradation, cellular infiltration, and extracellular matrix deposition within the scaffold [2-4]. This study investigates the development of a model system to evaluate the remodeling of implanted collagen scaffolds using MRI and conventional histological techniques.

Methods: The scaffolds were prepared from insoluble bovine collagen as described in [5]. Three types of sponges were fabricated from this starting material: 1.) one type was crosslinked with 1-ethyl-3-(3-dimethyl aminopropyl) carbodiimide (EDC) to increase resistance to biodegradation; 2.) for the second type, chondroitin 6-sulphate (CS) was used with EDC (EDC+CS) to increase the biocompatibility of the sponge, and; 3.) the third type was hydrated in MES buffer only and designated as uncrosslinked (UNX). Each sponge type was implanted in dorsal subcutaneous pockets of Sprague-Dawley rats (n=8). Two days after surgery and then weekly for up to 6 weeks, MRI experiments were performed at 2.0T to image the sponges. Multi-slice T_2-weighted images were acquired with the following parameters: TR=2500ms, 12 echo times from TE=12–144ms, FOV=6cm×4cm, matrix=256×128, slice thickness=2mm, NEX=2. Diffusion-weighted imaging (DWI) was performed using a spin-echo, echo-planar imaging pulse sequence with diffusion-sensitive gradient pulses (b values=15–760 mm^2s^{-1}) applied along three different gradient axes with gradient separation Δ=35ms and gradient duration δ=4ms. Other parameters were: TR/TE=2000ms/53ms, matrix=64×64, slice thickness=2mm, NEX=2. T_2 maps and apparent diffusion coefficient (ADC) maps were generated from T_2- and diffusion-weighted images. Animals were euthanized and sponges were harvested at each of the imaging time points. Histology was performed using Heamotoxylin & Eosin (H&E) and Masson's trichrome. Cellular infiltration and void area fraction of each scaffold was quantified to determine cellular density and overall tissue growth into the scaffolds, respectively. These histological measurements and the MRI parameters were explored in various combinations to check for correlations.

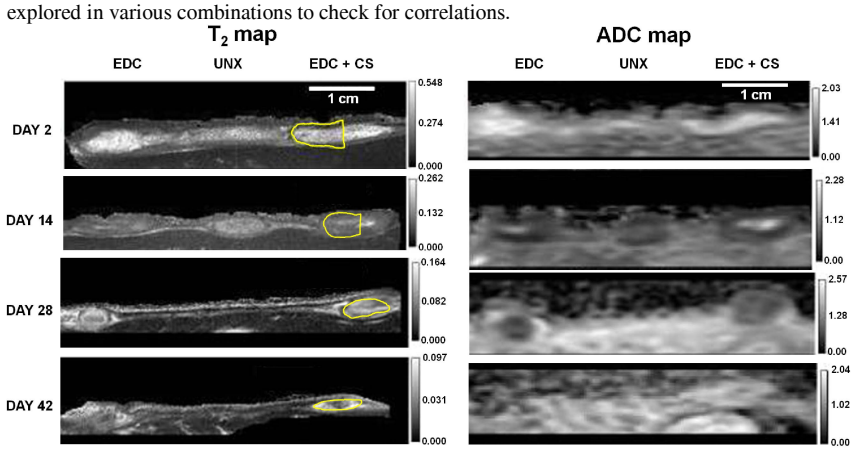

Fig. 1 – T_2 and ADC maps of three different implants (EDC, UNX, and EDC+CS) shown at different time points after implantation. T_2 map scale-bar values are in seconds and ADC map scale-bar values are ADC×10^{-5} cm^2/s. Yellow demarcations in T_2 map correspond to approximate location of histological sections shown in Fig. 2.

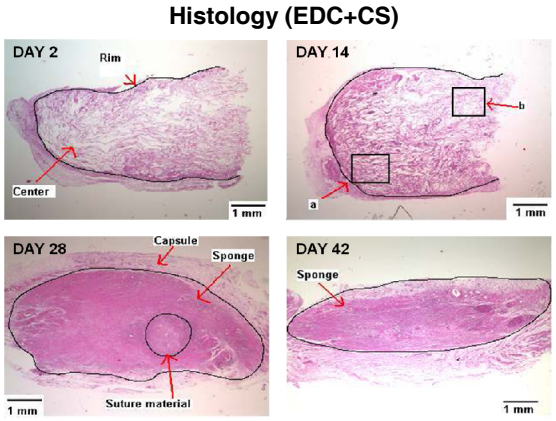

Fig. 2 – H&E histological section of EDC+CS sponge shown in different days following implantation. (a) and (b) on Day 14 indicate regions of cellularity and porosity, respectively.

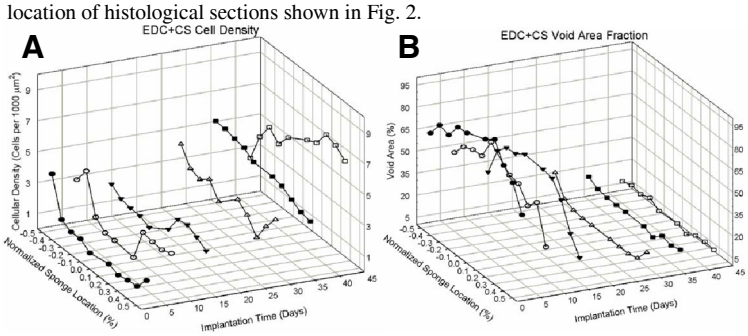

Fig. 3 – Plots of cellular densities (**A**) and void area fractions (**B**) for EDC+CS scaffolds as a function of scaffold location and implantation time.

Results and Discussion: On Day 2, the UNX sponges showed lower water T_2 and water ADC values compared to both crosslinked sponges due to its less-porous structure. Calculated T_2 and ADC maps showed a homogeneous center within each sponge surrounded by a thin rim with little or no integration between sponges and surrounding tissue. The H&E section from the EDC+CS sponge showed lattice-like lamellae appearing to form a highly porous interconnecting network with a rim comprised of a thin layer of infiltrated cells (Fig. 2). With the progression of time the volume of all sponges decreased with the sponges exhibiting more heterogeneous and lower T_2 and ADC values (Fig. 1). The H&E sections of EDC+CS sponges showed the sponge rim with a high degree of cellular infiltration and the sponge center showed little remaining porous structure on Day 14, which progressively became more homogeneous at later time points with complete cellular infiltration and integration with surrounding tissues (Fig. 2). The implants were surrounded by capsules which showed lower ADC values compared to the center of the sponges (Days 14 and 28). UNX sponges were completely degraded by Day 28 as confirmed by the MRI parameter maps (Fig. 1). EDC sponges degraded more rapidly compared to EDC+CS sponges. Cellular density, measured from the histological images, showed increasing trend in cell numbers with increasing time for all scaffolds (EDC+CS in Fig. 3A). All scaffolds showed a decrease in the void fraction with increasing implantation time (EDC+CS in Fig. 3B). Pearson's *r* was computed for different combinations of MRI and histology parameters from all time points (Table 1). These results indicate a statistical significant ($p<0.05$) linear relationship between the calculated parameters with void area and T_2 showing the best correlation while cell density and ADC showed the weakest correlation.

	n = 21	MRI parameter	
		T_2	**ADC**
Histology parameter	**Cell density**	r = -0.50 p = *0.02*	r = -0.46 p = *0.04*
	Void area	r = 0.67 p<*0.0001*	r = 0.50 p = *0.02*

Table 1 – Correlation statistics summary

Conclusion: Correlations in Table 1 show statistically significant relationships between cellular density, void area, T_2 and ADC measurements demonstrating that MRI is sensitive to specific remodeling parameters. Understanding the relationship between histology and MRI parameters can help guide the interpretation of MRI data as well as to reliably detect changes within implants using MRI data alone, reducing the need for scaffold harvesting and destructive testing.

References: [1] Hong *et al*. (2006). Tissue Eng **12**:843-854; [2] Packer (1977). Phil Trans R Soc Lond **278**:59-87; [3] Woerly *et al*. (2000). Tissue Eng **6**:265-278; [4] Viljanto *et al*. (1999). Wound Repair Regen **7**:119-126; [5] Pieper *et al*. (2000). Biomater **21**:1689-1699.